Multiband character revealed from weak antilocalization in platinum thin films

Subhadip Jana,[1,2,*] T. Senapati,[3,2] K. Senapati,[3,2] and D. Samal[1,2,†]
[1]*Institute of Physics, Bhubaneswar 751005, India*
[2]*Homi Bhabha National Institute, Anushakti Nagar, Mumbai 400094, India*
[3]*School of Physical Sciences, National Institute of Science Education and Research, Bhubaneswar 752050, India*

(Received 22 July 2022; revised 20 December 2022; accepted 22 December 2022; published 17 January 2023)

Platinum (Pt) has been very much used for spin-charge conversion in spintronics research due to its large intrinsic spin-orbit interaction. Magnetoconductance originating from weak antilocalization in the quantum interference regime is used as a powerful tool to obtain the microscopic information of spin-orbit interaction and the coherence phase breaking scattering process among itinerant electrons. To acquire the knowledge of different types of scattering processes, we have performed a magnetoconductance study on Pt thin films which manifests multiband (multichannel) conduction. An extensive analysis of quantum-interference-originated weak antilocalization reveals the existence of strong (weak) interband scattering between two similar (different) orbitals. Coherence phase breaking lengths (l_ϕ) and their temperature dependence are found to be significantly different for these two conducting bands. The observed effects are consistent with the theoretical prediction that there exist three Fermi sheets with one *s* and two *d* orbital character. This study provides the evidence of two independent nonsimilar conducting channels and the presence of anisotropic spin-orbit interaction along with *e-e* correlation in Pt thin films.

DOI: 10.1103/PhysRevB.107.035127

I. INTRODUCTION

Gaining control over the electron spin degree of freedom is very desirable in the field of spintronic research [1,2]. In recent days, spin-orbit interaction (SOI) has been found to provide a promising strategy for electrical manipulation of spin and magnetism in spintronic devices [3–6]. This includes the creation of spin current from the transverse charge current known as spin Hall effect (SHE) [7–9], and the exertion of a torque on a local magnetization from electrical current by the spin-orbit torque effect [10–13]. At a microscopic level, the asymmetric spin dependent electron scattering induced by SOI lies at the heart of the above phenomena [14,15]. Besides, a broader implication of SOI is realized in the design of topological materials with their potential use in low-energy dissipation and faster magnetization switching [16–19]. Materials with high-Z elements (Z is atomic number) are ideal candidates to look for spin-orbit interaction induced phenomena (SOI strength $\propto Z^4$ [20]). In particular, the 5*d* transition metal Pt has drawn lot of attention for spin-charge conversions and spin-torque effect in Pt/magnetic layer based heterostructures due to its intrinsic high SOI [21–24]. Further, the observation of the inverse spin Hall effect (ISHE) (reverse process of SHE, i.e., creation of charge current from transverse spin current) in $Ni_{81}Fe_{19}$/Pt and in Pt wire at room temperature provided an effective way to detect spin current [25,26]. In view of the extensive use of Pt in spintronics owing to its chemical inertness, easy fabrication of devices and most importantly strong intrinsic spin-orbit interaction, it is important to have a comprehensive understanding of spin-orbit interaction on electronic transport in bare metallic Pt thin films.

Quantum-interference-originated weak localization (WL) or weak antilocalization (WAL) is very much sensitive to the spin-orbit interaction (SOI) scattering process in conducting systems [27]. In real system, any type of deviation from perfect crystalline structure acts as a source of scattering potential for itinerant electrons. Scattered electrons propagating along time-reversed, identical self-intersecting trajectories known as a "Cooperon loop" (CL) [28,29] interfere constructively/destructively to give rise to suppression (WL)/enhancement (WAL) of conductivity. Experimentally, WL/WAL is usually determined from conductance correction to classical Drude conductivity at low temperature and in the presence of external magnetic field. The interference correction tends to vanish for most trajectories after averaging over the random scattering potentials, except for those scattered electrons which propagate in CL.

The application of uniform external magnetic field breaks the time-reversal symmetry required for the interference effect and induces an additional relative phase shift (due to enclosed magnetic flux) between the two electrons traversing CL. This effect suppresses constructive/destructive interference; as a result conductance gets enhanced (positive)/decreased (negative) with application of magnetic field in the WL/WAL regime [30,31]. Therefore, variation of magnetoconductance is used as a sensitive probe to detect the quantum interference effect. Traditionally, the manifestation of WAL has been attributed to SOI in material. In order for WAL to occur, it is crucial to have a π phase shift between two electron trajecto-

*subhadip.j@iopb.res.in
†dsamal@iopb.res.in

ries. The rotation of a spin-1/2 particle by 4π is equivalent to the identity operation and for most of the conducting systems, SOI gives rise to 2π rotation of itinerant electron spin which induces π phase shift resulting in the WAL effect [32,33]. Though Pt has been reported to exhibit the SOI-induced WAL effect [34], our work here is fundamentally different as it delves into understanding the importance of various electron scattering processes, multiband effects, orbital symmetry associated interband scattering, and *e-e* correlation on the electron transport properties (quantum interference regime) in Pt thin films.

In this work, we have carried out an in-depth magnetotransport study to examine the underlying SOI scattering of itinerant electrons from the WAL effect in Pt thin films. It is realized that SOI scattering strength [proportional to the characteristic spin-orbit magnetic field ($B_{so} \sim 2$ T)] is very much stronger than the coherent phase breaking scattering strength ($B_\phi \sim 0.004$ T at 2 K). The corresponding B_{so} and B_ϕ are extracted by using the Hikami-Larkin-Nagaoka (HLN) equation [Eq. (7)]. The corresponding spin-orbit scattering length l_{so} ($B_{so} = \hbar/4el_{so}^2$) for quasi-2D Pt thin film in the present study is estimated to be $l_{so} \sim 9$ nm ($B_{so} \sim 2$ T), which is close to the value $l_{so} \sim 12$ nm obtained for quasi-1D Pt nanowire from weak-antilocalization measurements, and it was comparable to the spin diffusion lengths determined from lateral spin valve ones [34].

Further, it has been found that the single conduction channel cannot be fitted well with experimental data; rather two independent conduction channels need to be considered to reconcile with experimental data. To get more information about conducting channels and their orbital symmetry, we examined the temperature-dependent behavior of B_ϕ. It is found that $B_\phi^1(T)$ for one channel exhibits prominent temperature dependence whereas $B_\phi^2(T)$ corresponding to the other channel shows weak temperature dependence. The observed difference in the temperature variation of $B_\phi^1(T)$ and $B_\phi^2(T)$ is attributed to two conducting channels made of orbitals with different symmetry. The bands originating from more symmetric orbitals are less sensitive to disorder whereas the bands originating from anisotropic orbitals are more sensitive to disorder and this is reflected in temperature-dependent $B_\phi^1(T), B_\phi^2(T)$. The observed effects are consistent with the theoretical prediction that there exist three Fermi sheets (FSs) with one *s* and two *d* orbital character [35–37]. This study provides the evidence of two independent nonsimilar conducting channels [one channel is made of the *s* orbital FS and other originates from combining two *d* orbital FSs (illustrated in Fig. 7)] and the presence of anisotropic spin-orbit interaction along with *e-e* correlation in Pt thin films.

II. EXPERIMENT

Platinum thin films were grown on Si/SiO_2 substrates using DC magnetron sputtering at room temperature with a base pressure 5×10^{-8} mbar. Before deposition, photolithography patterning with a Hall bar geometry was done with a mask aligner MDA-400M-N on 5×5 mm^2 substrates. The thickness variation of the Pt layer was achieved from a single deposition run by rotating the substrate plate holder. The structural characterization was carried out using a high-resolution x-ray diffractometer. The films were found to be polycrystalline with grains mainly grown/oriented on the (111) plane. The thickness of the films was determined to be 16 nm and 23 nm with a roughness about 3 Å from x-ray reflectivity (XRR) measurement. The magnetotransport measurements were performed in a cryogenic physical property measurement system (PPMS) with magnetic fields applied parallel and perpendicular to the film surface. We used Keithley 6221 as the current source and a Keithley 2182A nanovoltmeter for better data resolution.

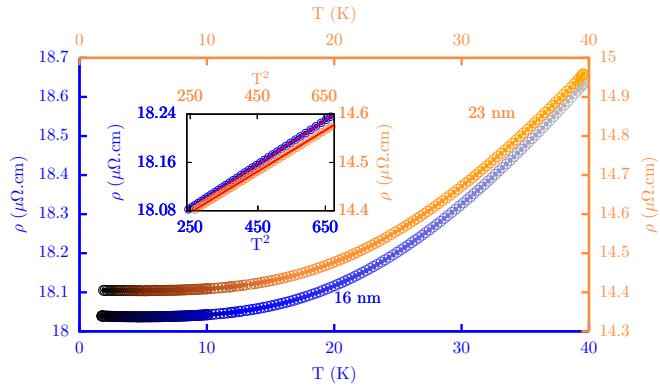

FIG. 1. Resistivity $\rho(T)$ vs T plot for Pt 16 nm (blue color) and 23 nm (orange color) films; darker color at low temperature indicates quantum interference regime. EEI-originated $\rho(T) \propto T^2$ in the temperature range 15 K $< T <$ 26 K is illustrated in inset [solid red color lines represent fitting of Eq. (1)].

III. RESISTIVITY AT LOW TEMPERATURE

The temperature-dependent resistivity ρ for 16 and 23 nm thick films (Fig. 1) exhibits a positive temperature coefficient ($\frac{d\rho}{dT} > 0$) above 6 K indicating metallic character. Moreover, in the intermediate temperature range 15 K $< T <$ 26 K, the resistivity follows quadratic temperature dependence which is attributed to *e-e* Coulomb interaction (EEI) [38–40] and is shown in inset of Fig. 1. Experimental data in the temperature range 15 K $< T <$ 26 K fits well with Eq. (1),

$$\rho(T) = \rho_0 + A_{\mathrm{FL}}\, T^2, \tag{1}$$

where ρ_0 is residual resistivity and A_{FL} accounts for the EEI contribution. From fitting, we obtain A_{FL} equal to 3.6×10^{-4} μΩ cm K^{-2} and 3.36×10^{-4} μΩ cm K^{-2} for 16 nm and 23 nm thick films, respectively. The obtained value of A is higher for 16 nm film as compared to 23 nm and it is consistent with theory that $A_{\mathrm{FL}} \propto E_F^{-2} \propto (m^*)^2$, where E_F and m^* are Fermi energy and effective mass of the electron, respectively [41]. The extracted values of A_{FL} are slightly higher than the reported value of $A_{\mathrm{FL}} \sim 10^{-5}$ μΩ cm K^{-2} for bulk Pt [40], which could be due to reduction of system dimension.

In the low-temperature regime (2 K $< T <$ 6 K), $\rho(T)$ exhibits an upturn which is attributed to the combined effect of quantum interference (WL/WAL) and EEI correction in the quasi-2D limit. This regime is denoted by the dark color shown in Fig. 1 and it is discussed in Sec. IV in terms of sheet conductance correction.

IV. SIGNATURE OF WAL EFFECT FROM TEMPERATURE-DEPENDENT SHEET CONDUCTANCE

At low temperature due to weak thermal agitation, electrons are able to move longer distance (on an average) with maintaining phase coherence which is known as phase coherence length (l_ϕ). Quantum interference manifests prominently when phase coherence length is very much longer than the mean-free path (l_e) of electrons ($l_\phi \gg l_e$). One of the indications of quantum interference correction is $\ln(T)$ dependence of sheet conductance ($\Delta\sigma_{QI}$) in the 2D limit ($l_\phi > t$, where t is film thickness) and in general, for N independent conducting channels or Fermi sheets, $\Delta\sigma_{QI}$ can be expressed as [43–45]

$$\Delta\sigma_{QI}(T) = N\gamma_{\rm int}\alpha p\frac{e^2}{2\pi^2\hbar}\ln(T/T_0), \tag{2}$$

where $\gamma_{\rm int}$ is related with interaction coupling strength among independent Fermi sheets (strong coupling and zero coupling lead to $N\gamma_{\rm int} \sim 1$ and $N\gamma_{\rm int} \sim N$, respectively), p is related with the temperature exponent of phase coherence length ($l_\phi^2 \propto T^{-p}$ [46–48]), T_0 depends on l_e, and α takes different values depending upon the dominant scattering process involved. For three extreme situations α follows as (i) $\alpha \sim -1/2$ in strong spin-orbit scattering with absence of magnetic impurity scattering (WAL), (ii) $\alpha \sim 1$ in the quantum coherent regime ($l_\phi > l_e$) in absence of spin-orbit and magnetic impurity scattering (WL), and (iii) $\alpha \sim 0$ in strong magnetic impurity scattering (which drives toward the classical scenario) [43]. Therefore, the coefficient of $\ln(T)$ in Eq. (2), $A_{QI} = N\gamma_{\rm int}\alpha p\frac{e^2}{2\pi^2\hbar}$, contains crucial information about the microscopic scattering process. Further, the EEI contribution to sheet conductance ($\Delta\sigma_e$) exhibits also similar $\ln(T)$ dependence. For N independent channels in the 2D limit, it can be expressed as [49–53]

$$\Delta\sigma_e(T) = N\frac{e^2}{2\pi^2\hbar}(2-2F)\ln(T/T_e), \tag{3}$$

where F is the averaged screened Coulomb interaction over the Fermi surface, normalized with zero momentum transfer in the EEI scattering process. Therefore, total correction to ($\sigma_{\rm total}$) can be expressed as

$$\Delta\sigma_{\rm total}(T) = A\frac{e^2}{2\pi^2\hbar}\ln(T/T'), \tag{4}$$

where $A = N[\gamma_{\rm int}\alpha p + (2-2F)]$ and T' is a constant.

Hence, it is not straightfoward to extract the value of α from zero magnetic field $\Delta\sigma(T)$ vs $\ln(T)$ experimental data, when the contributions from quantum interference and EEI coexist. To overcome this issue, one needs to exploit the temperature dependence of sheet conductance at constant weak magnetic fields since it will suppress mainly quantum interference contribution.

The quantum interference effect (WL/WAL) originates from particle-particle channel interaction between two electrons traversing in a "Cooperon loop" (CL) and it is very much sensitive to enclosed magnetic flux through the CL due to applied external magnetic field. However, the EEI effect is governed by the particle-hole channel interaction and it is not influenced by external weak magnetic field [49] (EEI can be influenced in higher magnetic field if $g\mu_B B > 1/\tau_{so}$, where

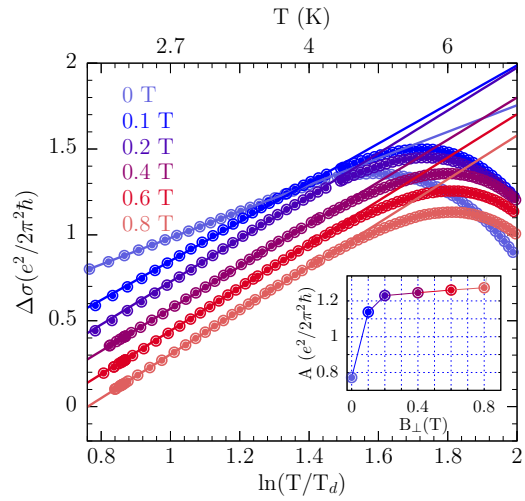

FIG. 2. Sheet conductance (relative change) $\Delta\sigma(T)$ vs $\ln(T/T_d)$ is plotted at different constant perpendicular magnetic fields ($0 \leqslant B_\perp \leqslant 0.8$ T) for Pt 16 nm thick film. Solid lines represent the fitting of $\Delta\sigma(T)$ vs $\ln(T/T_d)$ using Eq. (4) in the low-temperature regime. (The upper x axis denotes the real temperature and $T_d = 1$ K [42]; vertical offsets to plots are given for clarity.) The extracted coefficient A for different $B_\perp$ is shown in the inset.

τ_{so}, g, and μ_B are SOI scattering time, Landé g factor, and Bohr magneton, respectively) [44,53–57]. As a consequence of the above fundamental differences between quantum interference effect (WL/WAL) and EEI, one can disentangle the WL/WAL and EEI contributions by applying (perpendicular to the film surface) constant weak external magnetic fields. The applied field will suppress the WL/WAL contribution, while the EEI effect remains unaffected. Hence, the change in the $\ln(T)$ coefficient upon the application of weak magnetic field will provide only the WL/WAL contribution [i.e., A_{QI} in Eq. (2)].

We investigated the variation of the $\ln(T)$ coefficient (A) in $\sigma(T)$ with applying constant perpendicular external magnetic fields ranging from 0 to 0.8 T, shown in Fig. 2. A systematic change in A was observed with the increment of external constant magnetic field and we obtained maximum change in $\ln(T)$ coefficient as $A_{QI} = A|_{B=0} - A|_{B=0.8} = -0.56$ (in quantum conductance unit, $e^2/2\pi^2\hbar$). To evaluate the value of α from A_{QI} that contains the information about the dominant scattering process, one requires to know the values of $N\gamma_{\rm int}$ and p. The p adapts a universal value depending upon the dominant interaction responsible for the inelastic scattering process in the system. In particular, for EEI-originated inelastic scattering, l_ϕ^{-2} ($l_\phi^{-2} \propto T^p$) exhibits linear temperature dependence at low temperature and it shows a crossover from T to $T^2\ln(T)$ behavior with the increment of temperature [48].

Two possible cases can be invoked to assess the value of α: (i) For Pt thin films, resistivity follows quadratic temperature dependence (14 K $< T <$ 23 K) (Sec. III) which signifies the dominance of electron-electron scattering over electron-phonon scattering; therefore, p can be approximated as $\sim$1 at lower temperature [45]. Considering single channel $N =$

1 or strong coupling interaction $N\gamma_{\rm int} \sim 1$, one can obtain $\alpha \sim -1/2$ [Eq. (2)]. (ii) Effective two independent channels with $N = 2$ and $p = 1$ [extracted from magnetoconductance analysis, Sec. V A, as extracted $B_\phi(T)$ follows straight line behavior with temperature from 2 K to 6 K] give rise to $\alpha \sim -0.28$ [Eq. (2)].

From detailed magnetotransport analysis (discussed in Sec. V), it is realized that the conduction takes place through two independent channels $N = 2$ in Pt thin films. Considering two channel conduction, Eq. (2) provides the value of $\alpha = -0.56/(N\gamma_{\rm int}p) = -0.56/(2 \times 1) \sim -0.28$ (as discussed above) which is very much unexpected for a highly spin-orbit coupled system. To find out the source of this discrepancy, we looked again into the explicit temperature dependence in the sheet conductance correction [Eq. (2)] due to the quantum interference effect. One can primarily visualize that with the increment of temperature, random thermal agitation enhances the inelastic scattering among itinerant electrons and as a consequence, l_ϕ becomes temperature dependent [explicit functional form is determined by the dominating scattering mechanism (*e*-*e*, *e*-phonon scattering) at nonzero temperature]. The l_ϕ fixes the upper cutoff spatial dimension for quantum interference effect and the interference originated correction is proportional to the available coherence area ($\propto l_\phi^2$). Thus, for a single channel with phase coherence length l_ϕ, $\Delta\sigma_{QI} \propto -\ln(l_\phi^2/l_e^2)$. On the contrary, dominant disorder induced inelastic scattering leads to temperature independent l_ϕ [58] and such kind of conducting channel cannot contribute to $\Delta\sigma_{QI}(T)$ considerably. Therefore, for a system with N nonsimilar independent conduction channels, $\Delta\sigma_{QI}(T)$ can be expressed as

$$\Delta\sigma_{QI}(T) = -\alpha \sum_{n=1}^{N} \frac{e^2}{2\pi^2\hbar} \ln\left[\left(l_\phi^n/l_e^n\right)^2\right]. \tag{5}$$

It has been observed from magnetoconductance analysis that the examined Pt thin film possesses two independent conducting channels, one of which shows prominent temperature dependence [$B_\phi^1(T) \propto T$; Fig. 4(b)] at lower temperature regime (2 K $< T <$ 6 K), and $B_\phi^2(T)$ associated with other channel follows a negligible logarithmic temperature variation in comparison with $B_\phi^1(T)$ (detailed description is given in the Supplemental Material [59]). This implies that the contribution to the slope of $\ln(T)$ [Eq. (5)] from the second channel is negligible. Thus, Eq. (5) can effectively be converted into

$$\begin{aligned}\Delta\sigma_{QI}(T) &= -\alpha\frac{e^2}{2\pi^2\hbar}\left(\ln\left(l_\phi^1/l_e^1\right)^2 + \ln\left(l_\phi^2/l_e^2\right)^2\right)\\ &= -\alpha\frac{e^2}{2\pi^2\hbar}\left(\ln\left[l_\phi^1(T)/l_e^1\right]^2 + \ln\left[l_\phi^2(T)/l_e^2\right]^2\right)\\ &\sim \alpha\frac{e^2}{2\pi^2\hbar}\left(\ln\left(T/T_0^1\right) + c\right),\end{aligned} \tag{6}$$

where c is a temperature-independent constant as l_ϕ^2 exhibits negligible temperature dependence. Since only one channel contributes (logarithmic temperature correction) to $\Delta\sigma_{QI}(T)$, we obtained $\alpha = -0.56/(N\gamma_{\rm int}p) = -0.56/(1 \times 1) \sim -1/2$ which is consistent with the theoretical value of α in the presence of strong spin-orbit scattering.

We now turn to the estimation of EEI strength which is related with screened Coulomb potential F. For strong interaction, F is a small fractional number and for free electrons $F \sim 1$. F can be evaluated by considering that at a magnetic field of 0.8 T, the quantum interference effect becomes very much weaker [60] and then one can approximate the coefficient $A|_{B=0.8\rm T} \sim N \times 2(1 - F) = 1.22$ ($N = 2$ as discussed before), which leads to $F \sim 0.7$. The $5d$ correlated transition metal Pt exhibits a higher value of F which indicates that the *e*-*e* Coulomb interaction is weaker in comparison with the strongly electron correlated $3d$ transition metal Cu $F_{Cu} \sim 0.5$ [61].

V. WAL EFFECT FROM MAGNETIC FIELD VARIATION

A. Perpendicular magnetic field ($B_\perp$)

The magnetotransport measurement is a powerful tool to extract different types of microscopic scattering lengths (i.e., spin-orbit, inelastic scattering) by exploiting the quantum-interference-originated correction (WAL/WL) to sheet conductance. The quantum interference effect (WL/WAL) manifests more prominently with the reduction of dimension. For a quasi-2D system (where phase coherence length (l_ϕ) is greater than film thickness (t) and detailed discussion is given in the Supplemental Material [59]) with N independent conducting channels, the variation of sheet conductance [$\Delta\sigma(B_\perp) = \sigma(B_\perp) - \sigma(0)$] with external perpendicular magnetic field ($B_\perp$) is described by the Hikami-Larkin-Nagaoka (HLN) equation which can be expressed as [43,53,62–64]

$$\begin{aligned}\Delta\sigma(B_\perp) = -\frac{e^2}{2\pi^2\hbar}\sum_{n=1}^{N}\Bigg[&\left\{\psi\left(1/2 + B_e^n/B_\perp\right) + \ln\left(B_\perp/B_e^n\right)\right\}\\ &+\frac{1}{2}\left\{\psi\left(1/2 + B_\phi^n/B_\perp\right) + \ln\left(B_\perp/B_\phi^n\right)\right\}\\ &-\frac{3}{2}\left\{\psi\left(1/2 + \frac{B_\phi^n + B_{so}^n}{B_\perp}\right) + \ln\left(\frac{B_\perp}{B_\phi^n + B_{so}^n}\right)\right\}\Bigg],\end{aligned} \tag{7}$$

where $\psi(x)$ is the digamma function, B_e^n, B_ϕ^n, and B_{so}^n correspond to characteristic magnetic fields of the nth channel which is related with scattering lengths (l_e, l_ϕ, and l_{so}) as $B_i = \hbar/4el_i^2$, where l_e, l_ϕ, and l_{so} denote elastic, phase coherence, and spin-orbit scattering lengths, respectively, and B_e is determined from the semiclassical approximation and detailed discussion is given in the Supplemental Material [59].

If independent channels are very much similar to each other, then the characteristic magnetic fields B_i^n corresponding to each channel are nearly equal and as a result the HLN equation (7) for N channels becomes

$$\begin{aligned}\Delta\sigma(B_\perp) = -N\frac{e^2}{2\pi^2\hbar}\Bigg[&\{\psi(1/2 + B_e/B_\perp) + \ln(B_\perp/B_e)\}\\ &+\frac{1}{2}\{\psi(1/2 + B_\phi/B_\perp) + \ln(B_\perp/B_\phi)\}\\ &-\frac{3}{2}\left\{\psi\left(1/2 + \frac{B_\phi + B_{so}}{B_\perp}\right) + \ln\left(\frac{B_\perp}{B_\phi + B_{so}}\right)\right\}\Bigg].\end{aligned} \tag{8}$$

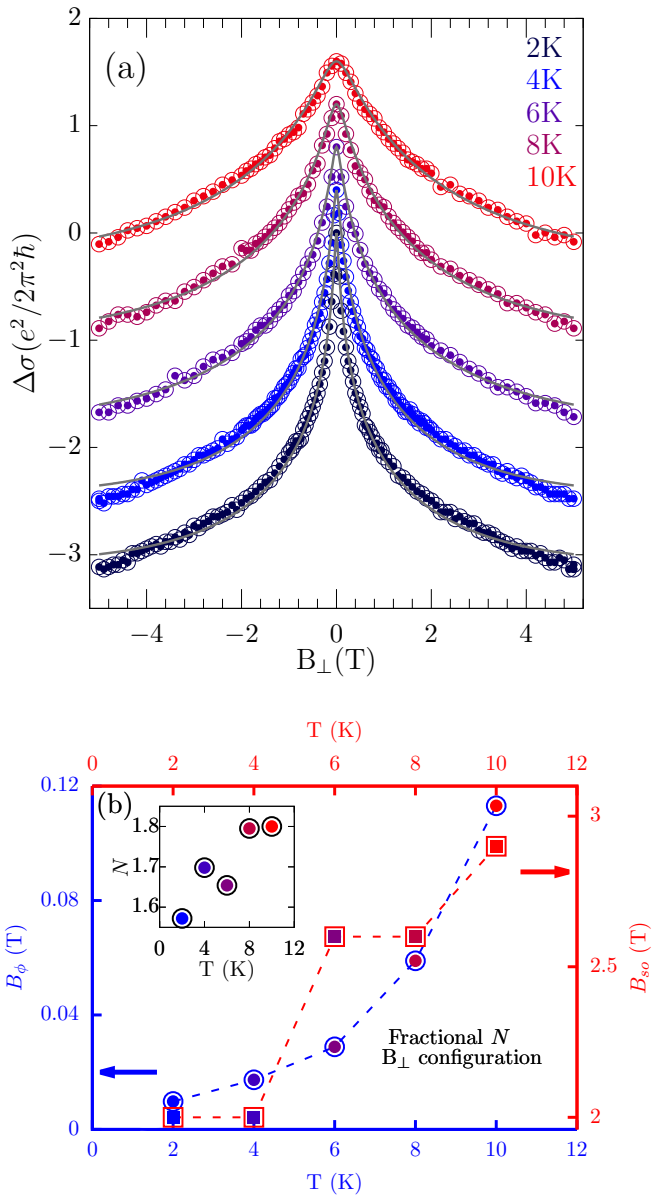

FIG. 3. (a) Magnetoconductance $\Delta\sigma(B_\perp)$ is fitted with HLN equation at different temperatures for 16 nm Pt film [solid gray color lines represent fitting of Eq. (8); vertical offsets to plots are given for clarity]. (b) Extracted B_ϕ, B_{so} are illustrated at different temperatures; inset displays the fractional value of N at various temperatures.

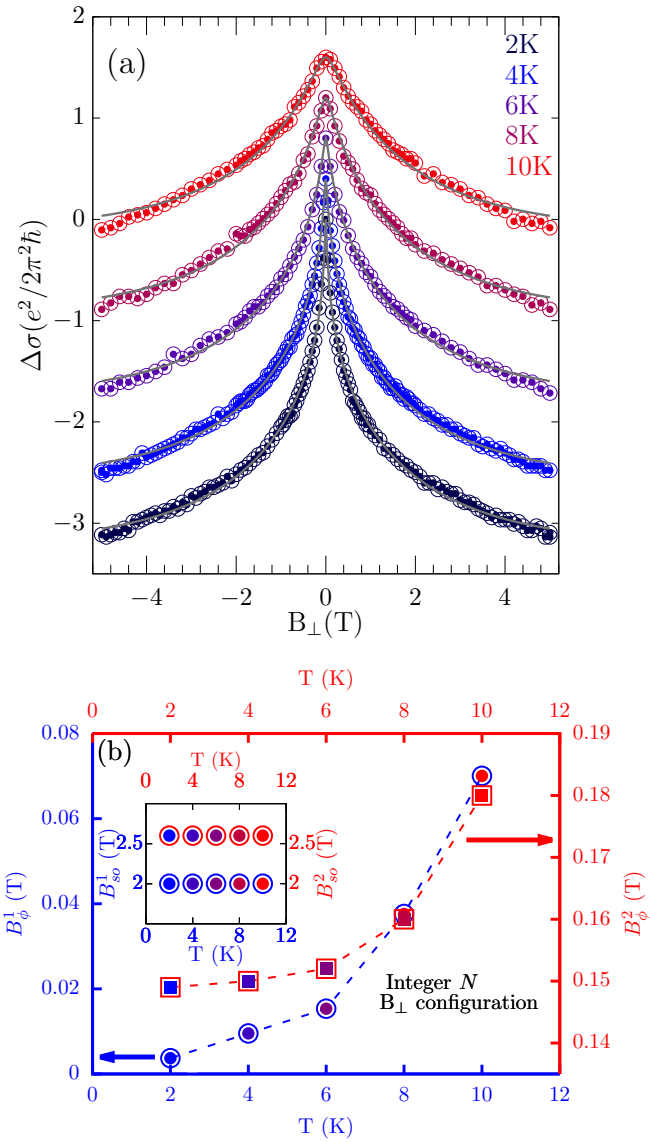

FIG. 4. (a) Magnetoconductance $\Delta\sigma(B_\perp)$ is fitted with HLN equation at different temperatures [solid gray color lines represent fitting of Eq. (7)] for 16 nm Pt film (vertical offsets to plots are given for clarity). (b) Extracted B^n_ϕ for two different independent channels ($n = 1, 2$) are illustrated at different temperatures; inset displays the value of B^n_{so} at various temperatures.

Figure 3(a) shows the sheet conductance variation with perpendicular magnetic field for 16 nm thick film at different temperature. The presence of a sharp cusp at lower temperature indicates the WAL effect. However, the sharpness disappears rapidly with the increment of temperature. Experimental data $\Delta\sigma(B_\perp)$ are fitted well with Eq. (8); nevertheless the fitting provides the fractional value of N which cannot be anticipated by considering independent conducting channels. The fitting and the corresponding best fitting parameters (B_ϕ, B_{so}, N) are illustrated in Figs. 3(a) and 3(b), respectively. The fractional value of N can appear due to the following reasons: (i) the presence of weak but non-negligible interorbital scattering among channels [65,66] and (ii) the channels possessing different sets of B^n_e, B^n_{so}, B^n_ϕ.

To obtain more meaningful insight about the conducting channels in Pt thin films, the magnetoconductance data are further analyzed by considering the more general equation [Eq. (7)] with the independent channels having different sets of B^n_e, B^n_{so}, B^n_ϕ. The fitting is shown in Fig. 4(a) and the best fitting parameters (B^1_ϕ, B^2_ϕ, B^1_{so}, B^2_{so}) are shown in Fig. 4(b) (for 16 nm thick Pt film). From the fitting, we obtain $N = 2$ and the phase coherence magnetic field ($B^1_\phi \sim 0.004$ T at 2 K) for one channel to be higher than the other ($B^2_\phi \sim 0.15$ T at 2 K). The phase coherence length (l_ϕ) is related with B_ϕ as $B_\phi = 1/4el^2_\phi$ and when the phase coherence length is larger than film thickness, the system is considered to be in

quasi-2D. In the present case, the quasi-2D limit is confirmed by making comparison between phase coherence length and film thickness and is shown in the Supplemental Material [59]. Further, the spin-orbit scattering magnetic fields $B^1_{so} \sim 2$ T, $B^2_{so} \sim 2.5$ T are found to be very much higher than both B^1_ϕ, B^2_ϕ. The obtained fitting parameters provide the following physical interpretations: (i) the Pt metal possesses large intrinsic spin-orbit interaction $B_{so} \sim 2$ T (in perpendicular configuration with integer number channels $N = 2$), (ii) the presence of two independent conducting channels in Pt thin film, and (iii) the logarithmic variation of $B^1_\phi(T)$ with temperature is very much prominent in comparison with $B^2_\phi(T)$ and $B^1_\phi < B^2_\phi$ (detailed description is given in the Supplemental Material [59]). The prominent variation of B^1_ϕ vs T for one channel indicates that the inelastic scattering process is dominated by possible *e-e* scattering (Sec. III). However, the other channel with weakly temperature-dependent inelastic scattering process (at low-temperature regime $2 < T < 6$ K) indicates that a significant amount of disorder scattering is present. To further examine the multiband character in 23 nm thick Pt film, we analyzed data in the same way as that of 16 nm thick Pt film and we found that $B^1_{so}, B^1_\phi, B^2_{so}$, and B^2_ϕ corresponding to 23 nm film also follow similar behavior with temperature variation. The fitting and obtained parameters for 23 nm film are illustrated in Figs. S2(a) and S2(b) of the Supplemental Material [59]. This indicates that the observed multiband effect is generic to Pt thin films.

B. Parallel magnetic field ($B_{||}$)

In quasi-2D systems, itinerant electrons can diffuse along film thickness by satisfying the restriction of quantum mechanical boundary conditions [62]. Hence, the quantum interference effect gets influenced even in parallel magnetic field configuration. The quantum-interference-originated magnetoconductance correction in the $B_{||}$ configuration for N independent channels is given by [45,62,67–69]

$$\Delta\sigma(B_{||}) = \frac{e^2}{2\pi^2\hbar}\sum_{n=1}^{N}\left[\frac{3}{2}\ln\left(1+\frac{B^2_{||}}{B_t\left(B^n_{so}+B^n_\phi\right)}\right) - \frac{1}{2}\ln\left(1+\frac{B^2_{||}}{B_t B^n_\phi}\right)\right], \quad (9)$$

where B_t is defined as $B_t = 12\hbar/et^2$ and t is film thickness.

For simplicity, if we assume all independent channels to have equal characteristic magnetic filed, then Eq. (9) gets modified as

$$\Delta\sigma(B_{||}) = N\frac{e^2}{2\pi^2\hbar}\left[\frac{3}{2}\ln\left(1+\frac{B^2_{||}}{B_t(B_{so}+B_\phi)}\right) - \frac{1}{2}\ln\left(1+\frac{B^2_{||}}{B_t B_\phi}\right)\right]. \quad (10)$$

Experimental data $\Delta\sigma(B_{||})$ are fitted well with Eq. (10) [Fig. 5(a)], but the fitting provides a fractional value of N. The extracted parameters are illustrated in Fig. 5(b) for 16 nm thick film. As previously we have discussed that the number of independent conducting channels cannot be a fractional value, different channels must have different characteristic magnetic fields. Therefore, we analyzed $\Delta\sigma(B_{||})$ considering the independent channels to have different sets of B^n_{so}, B^n_ϕ [Eq. (9)] which is shown in Figs. 6(a) and 6(b) for 16 nm thick Pt film. Similarly, for 23 nm thick Pt film, the data fitting and the best fitting parameters are shown in Figs. S3(a) and S3(b) of the Supplemental Material [59].

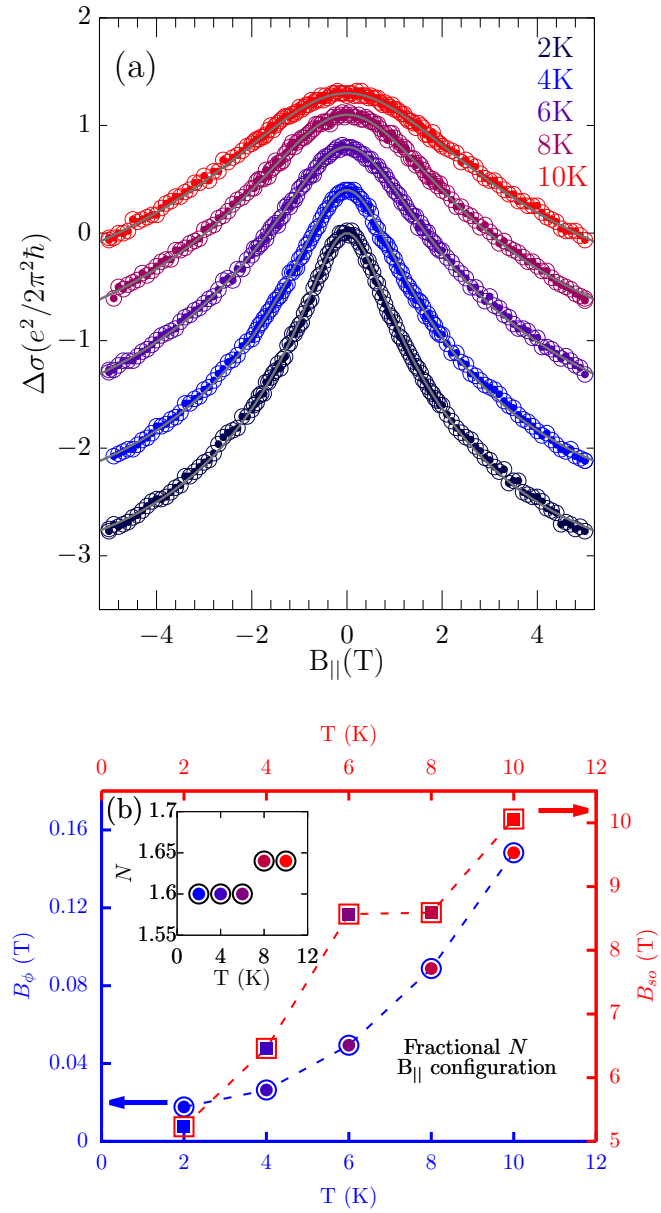

FIG. 5. (a) Magnetoconductance $\Delta\sigma(B_{||})$ is fitted with HLN equation at different temperatures for 16 nm Pt film [solid gray color lines represent fitting of Eq. (10); vertical offsets to plots are given for clarity]. (b) Extracted B_ϕ, B_{so} are illustrated at different temperatures; inset displays the fractional value of N at various temperatures.

In parallel magnetic field configuration, the extracted values of B^1_ϕ [by fitting with Eq. (9)] are found to be pretty close to B^1_ϕ obtained [by fitting with Eq. (7)] in perpendicular magnetic field configuration and follow very similar behavior with temperature. However, the obtained B_{so} are very different for perpendicular and parallel configurations. This confirms

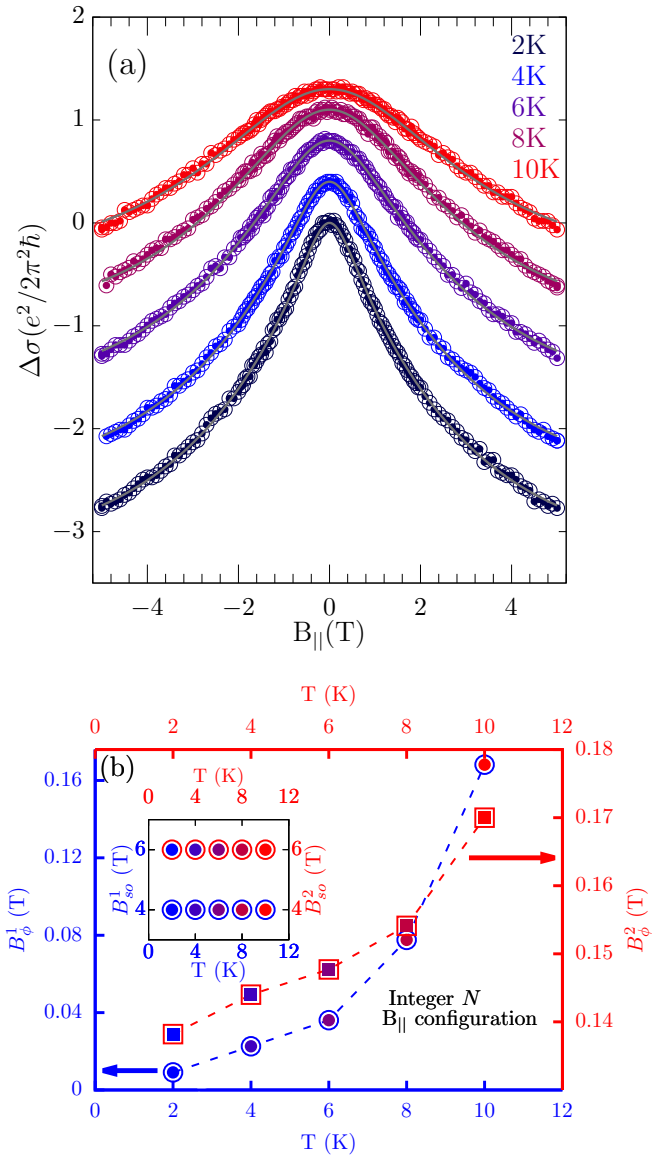

FIG. 6. (a) Magnetoconductance $\Delta\sigma(B_{||})$ is fitted with HLN equation at different temperatures [solid gray color lines represent fitting of Eq. (9)] for 16 nm Pt film (vertical offsets to plots are given for clarity). (b) Extracted B^n_ϕ for two different independent channels ($n = 1, 2$) are illustrated at different temperatures; inset displays the value of B^n_{so} at various temperatures.

the anisotropic nature of the spin-orbit scattering potential in Pt thin films.

VI. SUMMARY AND CONCLUSIONS

It was predicted from a theoretical band structure calculation that Pt metal (electronic configuration $5d^9 6s^1$) has three sheets of Fermi surfaces which are composed of s band and two from d band [36]. We realized the presence of two independent conduction channels from our magneto-transport analysis in both perpendicular and parallel magnetic configurations. This apparent discrepancy (theoretically three

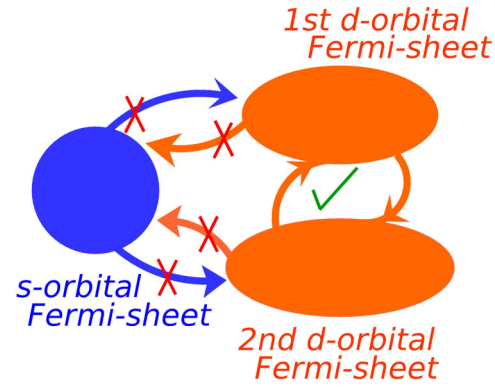

FIG. 7. The schematic diagram for theoretically predicated three Fermi sheets, one derived from s orbital (blue color) and the other two derived from d orbital (orange color). The possible interaction among them is denoted by arrows (allowed and forbidden interactions are marked by $\times$, $\checkmark$, respectively). Interconnected two d orbitals leads to one effective conducting channel and the other one is from s orbitals.

channels, experimentally two channels) leads to an insightful physics of orbital-symmetry-related interband scattering in Pt thin films. The two d-band channels are mixed up with each other due to their similar orbital nature and in the presence of intermixing scattering, they will act as an equivalent single channel. On the contrary, intermixing scattering among s, d band channels is very weak due to different orbital symmetry. As a result effectively there will be two independent conducting channels which is illustrated in Fig. 7. Second, we have found that the characteristic magnetic field for coherence phase breaking scattering (B^2_ϕ) corresponding to one channel shows a weak temperature dependence and this intriguing phenomenon could arise very often in a system with significant disorder scattering. However, B^1_ϕ for other the channel shows a prominent variation with temperature, indicating the presence of effectively weak disorder scattering. The crucial point is that the same amount of disorder in a system can act differently for different conduction channels depending upon its orbital symmetry. The bands derived from more anisotropic orbitals (e.g., d, p orbital) are very much sensitive to a minute amount of disorder [70,71] which can give rise to very high inelastic scattering in comparison to conducting channels made out of symmetric orbitals (e.g., s orbital).

To conclude, the symmetry of orbitals involved in conducting channels, the presence of EEI, and the anisotropic spin-orbit interaction are revealed from our magnetoconductance study in Pt thin films.

ACKNOWLEDGMENTS

S.J. and D.S. acknowledge financial support from Max Planck partner group. D.S. acknowledges funding support from SERB, Government of India (Grant No.: CRG/2019/005144). S.J. would like to thank R. Kumar for discussions.

[1] A. Fert, Rev. Mod. Phys. **80**, 1517 (2008).
[2] I. Žutić, J. Fabian, and S. Das Sarma, Rev. Mod. Phys. **76**, 323 (2004).
[3] S. Datta and B. Das, Appl. Phys. Lett. **56**, 665 (1990).
[4] J. Ryu, S. Lee, K.-J. Lee, and B.-G. Park, Adv. Mater. **32**, 1907148 (2020).
[5] S. Wolf, D. Awschalom, R. Buhrman, J. Daughton, S. von Molnar, M. Roukes, A. Y. Chtchelkanova, and D. Treger, Science **294**, 1488 (2001).
[6] J. Tian, S. Hong, I. Miotkowski, S. Datta, and Y. P. Chen, Sci. Adv. **3**, e1602531 (2017).
[7] M. I. D'Yakonov and V. Perel, JETP Lett. **13**, 467 (1971).
[8] M. I. Dyakonov and V. Perel, Phys. Lett. A **35**, 459 (1971).
[9] J. Sinova, S. O. Valenzuela, J. Wunderlich, C. H. Back, and T. Jungwirth, Rev. Mod. Phys. **87**, 1213 (2015).
[10] L. Zhu, D. C. Ralph, and R. A. Buhrman, Appl. Phys. Rev. **8**, 031308 (2021).
[11] X. Han, C. Wan, and G. Yu, Appl. Phys. Lett. **118**, 180401 (2021).
[12] C. Song, R. Zhang, L. Liao, Y. Zhou, X. Zhou, R. Chen, Y. You, X. Chen, and F. Pan, Prog. Mater. Sci. **118**, 100761 (2021).
[13] A. Manchon, J. Zelezny, I. M. Miron, T. Jungwirth, J. Sinova, A. Thiaville, K. Garello, and P. Gambardella, Rev. Mod. Phys. **91**, 035004 (2019).
[14] S. O. Valenzuela and M. Tinkham, Nature (London) **442**, 176 (2006).
[15] J. Wunderlich, B. Kaestner, J. Sinova, and T. Jungwirth, Phys. Rev. Lett. **94**, 047204 (2005).
[16] A. Mellnik, J. Lee, A. Richardella, J. Grab, P. Mintun, M. H. Fischer, A. Vaezi, A. Manchon, E.-A. Kim, N. Samarth *et al.*, Nature (London) **511**, 449 (2014).
[17] J. Puebla, J. Kim, K. Kondou, and Y. Otani, Commun. Mater. **1**, 24 (2020).
[18] T. H. Dang, J. Hawecker, E. Rongione, G. Baez Flores, D. Q. To, J. C. Rojas-Sanchez, H. Nong, J. Mangeney, J. Tignon, F. Godel, S. Collin, P. Seneor, M. Bibes, A. Fert, M. Anane, J.-M. George, L. Vila, M. Cosset-Cheneau, D. Dolfi, R. Lebrun, P. Bortolotti, K. Belashchenko, S. Dhillon, and H. Jaffres, Appl. Phys. Rev. **7**, 041409 (2020).
[19] L. Liu, C.-F. Pai, Y. Li, H. Tseng, D. Ralph, and R. Buhrman, Science **336**, 555 (2012).
[20] R. Meservey and P. M. Tedrow, Phys. Rev. Lett. **41**, 805 (1978).
[21] A. Magni, V. Basso, A. Sola, G. Soares, N. Meggiato, M. Kuepferling, W. Skowroński, S. Łazarski, K. Grochot, M. V. Khanjani, J. Langer, and B. Ocker, IEEE Trans. Magn. **58**, 4400205 (2022).
[22] G. Choi, J. Ryu, R. Thompson, J.-G. Choi, J. Jeong, S. Lee, M.-G. Kang, M. Kohda, J. Nitta, and B.-G. Park, APL Mater. **10**, 011105 (2022).
[23] L. Chen, K. Zollner, S. Parzefall, J. Schmitt, M. Kronseder, J. Fabian, D. Weiss, and C. H. Back, Phys. Rev. B **105**, L020406 (2022).
[24] G. G. B. Flores and K. D. Belashchenko, Phys. Rev. B **105**, 054405 (2022).
[25] E. Saitoh, M. Ueda, H. Miyajima, and G. Tatara, Appl. Phys. Lett. **88**, 182509 (2006).
[26] T. Kimura, Y. Otani, T. Sato, S. Takahashi, and S. Maekawa, Phys. Rev. Lett. **98**, 156601 (2007).
[27] G. Bergmann, Int. J. Mod. Phys. B **24**, 2015 (2010).
[28] J. Rammer, *Quantum Field Theory of Non-Equilibrium States* (Cambridge University Press, 2011), p. 349.
[29] P. Coleman, *Introduction to Many-Body Physics* (Cambridge University Press, 2015), p. 384.
[30] G. Bergmann, Phys. Rep. **107**, 1 (1984).
[31] F. V. Tikhonenko, A. A. Kozikov, A. K. Savchenko, and R. V. Gorbachev, Phys. Rev. Lett. **103**, 226801 (2009).
[32] G. Bergmann, Phys. Rev. Lett. **48**, 1046 (1982).
[33] E. McCann, Physics **2**, 98 (2009).
[34] Y. Niimi, D. Wei, H. Idzuchi, T. Wakamura, T. Kato, and Y. Otani, Phys. Rev. Lett. **110**, 016805 (2013).
[35] L. R. Windmiller, J. B. Ketterson, and S. Hornfeldt, J. Appl. Phys. **40**, 1291 (1969).
[36] J. B. Ketterson and L. R. Windmiller, Phys. Rev. B **2**, 4813 (1970).
[37] G. Y. Guo, S. Murakami, T.-W. Chen, and N. Nagaosa, Phys. Rev. Lett. **100**, 096401 (2008).
[38] W. De Haas and J. De Boer, Physica **1**, 609 (1934).
[39] M. J. Rice, Phys. Rev. Lett. **20**, 1439 (1968).
[40] A. Jacko, J. Fjaerestad, and B. Powell, Nat. Phys. **5**, 422 (2009).
[41] X. Lin, B. Fauqué, and K. Behnia, Science **349**, 945 (2015).
[42] Function $\ln(x)$ is not defined for dimensioned quantities. Therefore, to make the argument dimensionless, we use $\ln(T/T_d)$ as the x-axis label of Fig. 2 with $T_d = 1$ K.
[43] S. Hikami, A. I. Larkin, and Y. Nagaoka, Prog. Theor. Phys. **63**, 707 (1980).
[44] P. A. Lee and T. V. Ramakrishnan, Rev. Mod. Phys. **57**, 287 (1985).
[45] N. P. Breznay, H. Volker, A. Palevski, R. Mazzarello, A. Kapitulnik, and M. Wuttig, Phys. Rev. B **86**, 205302 (2012).
[46] B. L. Altshuler, A. G. Aronov, and D. E. Khmelnitsky, J. Phys. C: Solid State Phys. **15**, 7367 (1982).
[47] H. Fukuyama and E. Abrahams, Phys. Rev. B **27**, 5976 (1983).
[48] B. N. Narozhny, G. Zala, and I. L. Aleiner, Phys. Rev. B **65**, 180202(R) (2002).
[49] B. L. Altshuler, A. G. Aronov, and P. A. Lee, Phys. Rev. Lett. **44**, 1288 (1980).
[50] H. Fukuyama, J. Phys. Soc. Jpn. **50**, 3407 (1981).
[51] H. Fukuyama, J. Phys. Soc. Jpn. **51**, 1105 (1982).
[52] H. Fukuyama, J. Phys. Soc. Jpn. **50**, 3562 (1981).
[53] S. Jana, T. Senapati, and D. Samal, Phys. Rev. B **103**, 245109 (2021).
[54] B. L. Altshuler, D. Khmel'nitzkii, A. I. Larkin, and P. A. Lee, Phys. Rev. B **22**, 5142 (1980).
[55] P. A. Lee and T. V. Ramakrishnan, Phys. Rev. B **26**, 4009 (1982).
[56] P. Seiler, J. Zabaleta, R. Wanke, J. Mannhart, T. Kopp, and D. Braak, Phys. Rev. B **97**, 075136 (2018).
[57] A. Y. Kuntsevich, L. A. Morgun, and V. M. Pudalov, Phys. Rev. B **87**, 205406 (2013).
[58] K. Munakata, T. H. Geballe, and M. R. Beasley, Phys. Rev. B **84**, 161405(R) (2011).
[59] See Supplemental Material at http://link.aps.org/supplemental/10.1103/PhysRevB.107.035127 for the estimation of B_e, dimensionality of Pt films, temperature variation of B_ϕ^1, B_ϕ^2, and 23 nm thick film data analysis.
[60] The slope (A) of $\Delta\sigma_{\text{total}}(T)$ vs $\ln(T)$ changes (Fig. 2) ($\delta A \sim 0.05$) for the magnetic field variation from 0.6 T to 0.8 T. However, the same turns out to be $\delta A \sim 0.44$, for magnetic field variation from 0.0 T to 0.2 T.

[61] Y. Fehr, S. May-tal, and R. Rosenbaum, Phys. Rev. B **33**, 6631 (1986).
[62] B. Altshuler and A. Aronov, JETP Lett. **33**, 515 (1981).
[63] S. Jana, S. G. Bhat, B. C. Behera, L. Patra, P. S. A. Kumar, B. R. K. Nanda, and D. Samal, Europhys. Lett. **133**, 17005 (2021).
[64] L. Zhang, M. Dolev, Q. I. Yang, R. H. Hammond, B. Zhou, A. Palevski, Y. Chen, and A. Kapitulnik, Phys. Rev. B **88**, 121103(R) (2013).
[65] Two extreme situations, i.e., in the presence (absence) of strong interorbital scattering among N channels, give rise to an effective single channel (N channels) for magnetotransport phenomena. Therefore, intuitively a noninteger value of an independent channel may arise for intermediate (small but non-negligible) interorbital scattering strength.
[66] H. Nakamura, D. Huang, J. Merz, E. Khalaf, P. Ostrovsky, A. Yaresko, D. Samal, and H. Takagi, Nat. Commun. **11**, 1161 (2020).
[67] R. Rosenbaum, Phys. Rev. B **32**, 2190 (1985).
[68] R. S. Markiewicz and C. J. Rollins, Phys. Rev. B **29**, 735 (1984).
[69] W. C. McGinnis and P. M. Chaikin, Phys. Rev. B **32**, 6319 (1985).
[70] N. Mott, Philos. Mag. **17**, 1259 (1968).
[71] N. F. Mott, Philos. Mag. **19**, 835 (1969).